Eur. Phys. J. C (2025) 85:1389
https://doi.org/10.1140/epjc/s10052-025-15073-1

THE EUROPEAN PHYSICAL JOURNAL C

Regular Article - Experimental Physics

First measurement of GaAs as a scintillating calorimeter: achievements and prospects

A. Melchiorre[1,2,a], D. L. Helis[1,b], A. Puiu[1,c], G. Benato[1,3], P. Carniti[4], I. Colantoni[5,6], A. Continenza[2], N. Di Marco[1,3], A. Ferella[1,2], C. Ferrari[1,3], F. Giannessi[2], C. Gotti[4], E. Monticone[8], S. Nagorny[1,3], E. Olivieri[7], L. Pagnanini[1,3], G. Pessina[4], C. Petrucci[1,3], S. Pirro[1], A. Prajapati[1,2], G. Profeta[2], M. Rajteri[8], P. Settembri[2], A. Shaikina[1,3], C. Tresca[9], D. Trotta[4]

[1] INFN-Laboratori Nazionali del Gran Sasso, Assergi, 67100 L'Aquila, Italy
[2] Dipartimento di Scienze Fisiche e Chimiche, Università degli Studi dell'Aquila, 67100 L'Aquila, Italy
[3] Gran Sasso Science Institute, 67100 L'Aquila, Italy
[4] INFN and Università degli studi di Milano-Bicocca, 20126 Milan, Italy
[5] Consiglio Nazionale delle Ricerche, Istituto di Nanotecnologia, c/o Dip. Fisica, Sapienza Università di Roma, 00185 Rome, Italy
[6] INFN, Sezione di Roma, P.le Aldo Moro 2, 00185 Rome, Italy
[7] Université Paris-Saclay, CNRS/IN2P3, IJCLab, 91405 Orsay, France
[8] Istituto Nazionale di Ricerca Metrologica Torino, 10135 Turin, Italy
[9] CNR-SPIN, Università degli studi dell'Aquila, 67100 L'Aquila, Italy

Received: 2 July 2025 / Accepted: 13 November 2025

Abstract In this paper we present the first measurement of a Gallium Arsenide (GaAs) crystal as a scintillating calorimeter with dual heat and light readout within the DAREDEVIL project. The experimental setup features a 4.3 g GaAs (GaAs-1) crystal, operated at approximately 10 mK coupled with a Neutron Transmutation Doped (NTD) thermal sensor for phonon detection and an auxiliary calorimeter for the detection of scintillation light. For the GaAs-1 crystal, a baseline resolution of 121 ± 2 eV has been achieved. While, with a 3.5 g GaAs (GaAs-2) crystal an even better baseline resolution of 44.5 ± 0.8 eV was achieved. Alpha and X-ray calibration sources were used to study the scintillation light response to different types of interacting radiation. The GaAs crystal exhibits a strong particle discrimination capability based on the emitted scintillation light, featuring a light yield (LY) of 0.9 ± 0.2 keV/MeV for α induced events and 0.07 ± 0.01 keV/MeV for β/γ events, both measured at 1 MeV. The unusual luminescence behavior, i.e. more light being produced under irradiation by α particles warrants further investigation, particularly due to its potential to enhance sensitivity to low-energy nuclear recoils from light dark matter scattering.

[a] e-mail: andrea.melchiorre@lngs.infn.it (corresponding author)
[b] e-mail: dounia.helis@lngs.infn.it (corresponding author)
[c] e-mail: andrei.puiu@lngs.infn.it (corresponding author)

1 Introduction

The search for Dark Matter (DM), which constitutes approximately 27% of the universe's energy content, has driven innovative detection strategies in particle physics. Recently, one promising experimental approach was introduced for the direct DM detection through DM-electron scattering mechanism, which enables the exploration of sub-GeV DM candidates beyond traditional nucleon-based interactions [1,2]. Indeed, current efforts on a direct DM detection are primarily focused on Weakly Interacting Massive Particles (WIMPs) in the GeV–TeV range, with multi-ton-scale experiments such as LZ [3], XENONnT [4], DarkSide [5], and PANDA-X [6] pushing towards the so-called "neutrino floor" [7]. However, sub-GeV DM has gained increasing attention, with models such as asymmetric DM [8], freeze-in [9], and strong dynamics [10] expanding the search window down to eV-scale DM candidate particles [11]. The interaction between DM and electrons is particularly significant as it allows to access to lower mass DM candidates compared to the coherent nucleus scattering [12]. Recent results from XENONnT [13,14] have placed stringent constraints on DM-electron scattering cross-sections, demonstrating the power of electronic recoil detection in probing new parameter regions. Other experiments, including LUX [15], PANDA-X [6], and DarkSide-50 [16], have also shown sensitivity to sub-GeV DM, while DAMIC-M [17], EDELWEISS [18],

Published online: 06 December 2025

SENSEI [19], SuperCDMS [20], TESSERACT [21] and CRESST [22] have extended limits into the MeV/c^2 mass region. In this context, the DAREDEVIL project aims to develop a low-energy detection threshold, high-resolution cryogenic detector for future light DM candidates searches. The approach involves coupling state-of-the-art cryogenic sensors to materials with small or zero band gaps, such as semiconductors and Dirac/Weyl crystals [23–25], and operating them as cryogenic calorimeters [26]. Theoretical models suggest that low-mass DM may scatter off electrons, producing detectable electron recoils [12]. Extensive theoretical calculations [2] supports the potential of semiconductor-based detectors in uncovering interactions involving DM particles below the MeV/c^2 mass scale. A promising detector material for DM candidates in this mass region should combine several crucial properties:

1. use of a polar crystal, that would enhance sensitivity to dark photon absorption [27].
2. use of a semiconductor material, allowing for controlled and effective charge collection.
3. use of a scintillating material with an $\mathcal{O}$(eV) band gap (significantly smaller than NaI (5.86 eV) or CsI (3.5 eV)) [28] that will significantly increase the number of light photons emitted and improve the particle identification capability.

Gallium Arsenide (GaAs) is a particularly promising detector material due to its unique combination of physical and electronic properties, especially when used as a calorimeter at milliKelvin (mK) temperatures. Its direct band gap of approximately 1.42 eV [29] at room temperature is crucial for achieving high sensitivity to low-energy excitations, enabling the detection of sub-MeV DM particles through electron recoil processes. Moreover, GaAs is predicted to have a higher DM-electron fiducial cross-section compared to other low band gap semiconductors and metals [28]. It also outperforms other detector materials based on insulators for specific types of DM interactions, such as scattering mediated by dark photons or dark photon absorption [30,31]. As a polar material, GaAs is predicted to be particularly sensitive to DM interactions that involve optical phonons, dark photon mediators, or the Migdal effect [31–33].

The pure (undoped) GaAs crystal exhibits also a decent scintillating properties, producing 2 photons/keV under X-ray irradiation at 10 K [25]. Furthermore, recent studies demonstrate that GaAs scintillation properties could be further adjusted and enhanced through proper dopant selection [25,34]. Thereby, the GaAs material allows the implementation of a dual readout system, where both scintillation light and phonon signals are recorded simultaneously.

Indeed, to study the scintillation light one can use a Germanium light detector (Ge-LD), which consists of a thin (about 0.5 mm) high-purity germanium monocrystalline slabs, see for instance [35,36]. Scintillation photons interact with the LD and deposit their energy within its thin surface layer. Absorbed energy is subsequently converted into phonons, leading to a temperature increase of the system. Moreover, in order to further increase the sensitivity to the scintillation light, one can exploit the Neganov–Trofimov-Luke effect (NTL) on the Ge-LD. The NTL effect consists of the acceleration of primary electrons/holes produced under scintillation light and their further multiplication under the external bias (at the range of 50–100 V) that allows to amplify the phonon signal in Ge-LD without increasing the noise, i.e. improving the signal-to-noise ratio and lowering the energy threshold. Hence, applying a bias voltage to the Ge-LD enhances the particle discrimination capability and improves the sensitivity to rare events and weak light signals [37,38]. Therefore, this dual-readout system, combining phonon detection in GaAs and scintillation light measurement in can provide robust event-by-event particle identification, significantly reducing the misclassification of neutrons and alpha particles, from the electron/gamma events where the expected signal lies.

In the following paragraphs, we present the first measurements of the scintillation properties of GaAs at cryogenic temperature (around 10 mK) under illumination with X-rays and α particles over a wide energy range, together with its first demonstration as a dual-readout scintillating calorimeter. In addition, we report on the improved performance of GaAs in the phonon channel, which significantly enhances the sensitivity to low-mass DM candidates.

2 Experimental setup

Two GaAs single crystal wafers purchased from Sigma [39] were used as scintillating calorimeters in the present studies. Both wafers are 2-inch in diameter, but differ slightly in thickness - 0.5 mm (4.3 g, GaAs-1) and 0.325 mm (3.5 g, GaAs-2). The wafers were equipped with a 3×0.6×0.4 mm Ge-NTD [40] sensor using three epoxy glue spots onto the polished surface of the GaAs crystals. The GaAs wafers were then mounted with polytetrafluoroethylene (PTFE) clamps on a copper frame, as shown in Fig. 1.

Additionally, we used a Ge-LD a crystal with a diameter of 2-inch and a thickness of 0.5 mm for a total mass of 5.39g. We equipped the Ge-LD with the same type of Ge-NTD sensor as the GaAs wafers, attached to the surface of a Ge crystal in the same manner. The Ge-LD was mounted on a separate copper frame, fixed on the top of the GaAs detector frame, with a 10 mm separation between the two wafers. The Ge-LD electrodes, configured in a dot-circle pattern, for the NTL effect were bonded with 25 μm gold wires, which were connected to copper pins as shown in Fig. 2.

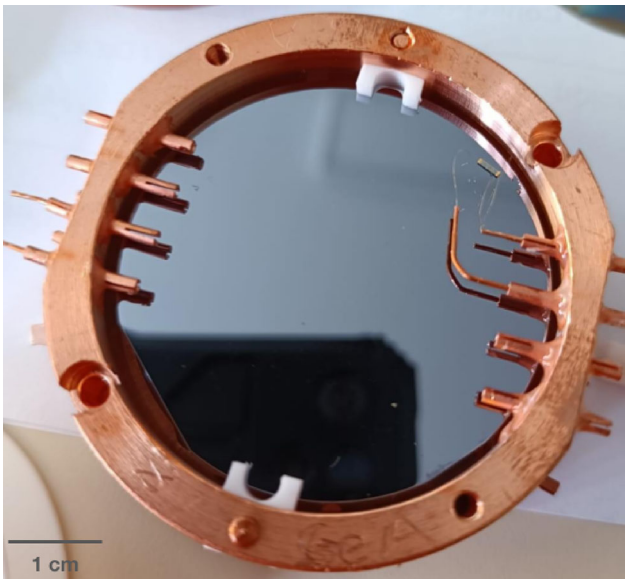

Fig. 1 The GaAs-1 detector mounted with PTFE clamps on the copper frame. On the right-hand side, the Ge-NTD thermistor is glued and connected via two 25-μm-thick gold wires to readout the heat signal. The whole frame was then coupled to the Ge-LD frame and to the 10 mK stage of the dilution refrigerator

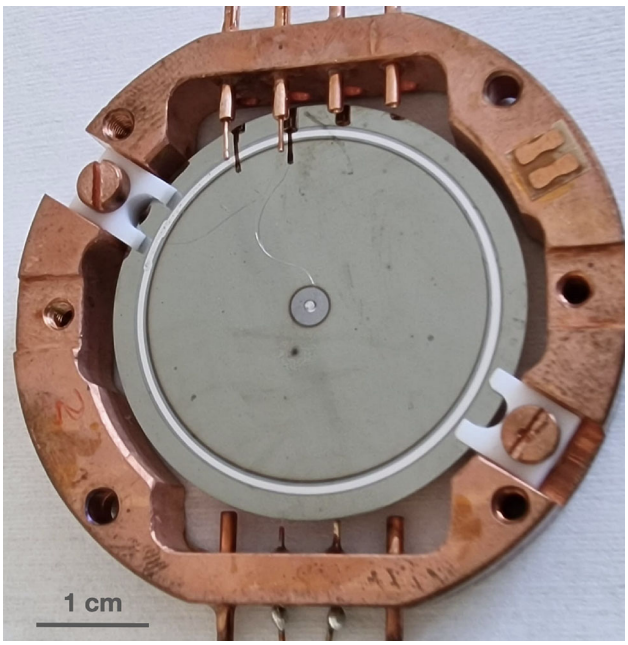

Fig. 2 The Ge light detector (Ge-LD) mounted with PTFE clamps on the copper frame. The image shows the electrodes for the NTL-effect, while the Ge-NTD thermistor is mounted on the opposite face and bonded with 25 μm gold wires, which were connected to copper pins. The entire frame was then coupled to the GaAs detector frame and to the 10 mK stage of the dilution refrigerator

Both detectors (GaAs and Ge-LD) were then thermally linked to the mixing chamber of a pulse-tube assisted dilution refrigerator (IETI) [41], located underground in Hall C at the Laboratori Nazionali del Gran Sasso (LNGS, Italy), and operated at a base temperature of 10 mK. Although the detector setup was operated underground at LNGS, it is important to emphasise that no specific selection of low-radioactivity materials was performed, and no additional shielding was used.

The electrical connection for the detector and for the bias voltage to the cryostat is established by connecting copper pins with constantan twisted wires to the thermalised board on the mixing chamber. The signal from the Ge-NTD's is then read out by an electronics unit positioned at room temperature. The room temperature readout electronics consist of low-noise DC-coupled front-end boards and high-resolution digitisers [42,43]. Signals from each detector were digitised with 24 bit ADC, followed by an anti-aliasing Bessel filter with a cutoff frequency of 500 Hz to eliminate higher-frequency noise, and synchronously recorded in a stream file using a MATLAB program [43].

In order to calibrate the detector energy response in the heat channel, a γ-ray source was employed, which consist of a Thorium tungstate (Th-W) wire, along with a ^{55}Fe X-rays source to illuminate the GaAs wafer with a total activity of approximately 1 Bq. This combination of γ-ray sources allows us to cover the calibration energy interval from 5.9 to 93 keV. Moreover, the detector setup was also equipped with a ^{238}U calibration α source with a smeared energy profile, similar to used in [44,45], that allows to irradiate the GaAs wafer with a 4.2 MeV and 4.8 MeV α particles to characterise its light response with respect to α irradiation. Similarly, for the energy calibration of the Ge-LD, was used a ^{55}Fe X-rays source with an activity of approximately 1 Bq. The geometry of the setup was arranged as follows: starting from the bottom, the ^{55}Fe source was placed facing, at a 5 mm distance, the electrode-free side of the Ge-LD, where the Ge-NTD sensor was mounted. Between the electrode side of the Ge-LD and the unpolished surface of the GaAs crystal, the α source was positioned to irradiate the GaAs. Finally, the polished GaAs face hosted the Ge-NTD sensor and faced both the ^{55}Fe source and the Th-W filament. In Table 1, the values of the electrical and acquisition parameters used in the measurement are reported.

3 Data analysis

The first level data analysis have been processed via a custom-made suite, written in Octave [46], which consisting of:

(1) The triggering software, based on a simple band-pass threshold algorithm, searches for the rising edge of the pulses recorded in the streaming. After data acquisition, the trigger selects events exceeding a threshold of 3 σ

Table 1 Summary of the electrical and acquisition parameters used in the measurements. The table reports the baseline and working resistances, the applied bias current, the sampling rate, and the trigger windows adopted for the GaAs and LD detectors

Parameter	GaAs	LD
R_{base}	272 MΩ	328 MΩ
R_{work}	2 MΩ	3 MΩ
Bias current	3.84 nA	3.84 nA
Sampling rate	10 kHz	10 kHz
Trigger window	120 ms	80 ms

above the baseline, and stores the time positions of each triggered event.

(2) Filtering processing program, based on the Gatti–Manfredi algorithm (Optimum filter OF) [47]. Each pulse window (defined around the trigger file positions) is filtered in the frequency domain via the OF transfer function and reconstructed in the time-domain: the maximum of the time-domain filtered signal event is taken as the energy estimator of the impinging particle. The transfer function is built by combining a template pulse (obtained by averaging several pulses in order to obtain a final pulse with S/N about 100) with the average Noise Power Spectrum, this latter built by averaging windows where no pulse was triggered. For each event several parameters are evaluated, i.e. rise-time, decay-time, time domain pulse-filtered χ^2. Multi-channel synchronised processing is made possible by using a common trigger file.

4 Results

4.1 GaAs-1 crystal

With the 4.3 g GaAs detector a 17-hour-long calibration run was performed. Compared to our previous results [48], we have improved the resolution of the GaAs detector in the heat channel by more than a factor of 2. Specifically, we can now clearly resolve the K_α and K_β peaks of the ^{55}Fe source as shown in inset of Fig. 3, achieving the energy resolution of $\sigma = 140 \pm 8$ eV for the peaks. This value was extracted from the fit of the spectrum using the sum of two Gaussian functions, one for the Mn K_α peak and one for the K_β peak, imposing the same sigma for both peaks. For the baseline resolution we obtained $\sigma_{RMS} = 121 \pm 2$ eV as reported in Table 2.

This was made possible by improvements to the cryostat, including the addition of a spring for further mechanical decoupling and an enhanced pulse tube support to reduce vibrational noise. Furthermore, from Fig. 3, we can observe

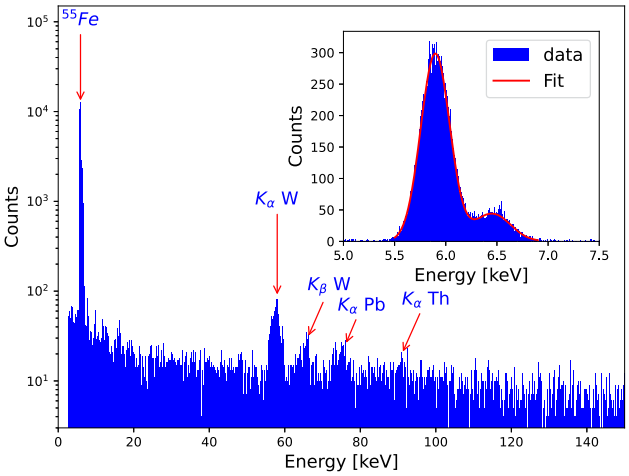

Fig. 3 X-ray energy spectrum acquired with the 4.3 g GaAs detector, showing the ^{55}Fe peak, the characteristic K_α/K_β lines of W, K_α lines of Pb and K_α lines of Th. The inset displays a zoomed view of the ^{55}Fe prominently featuring the 5.9 keV Mn K_α line and 6.49 keV Mn K_β

Table 2 Summary of the performance of GaAs-1 detector operated as a low-temperature calorimeter

Mass	4.3	g
Density	5.32	g/cm^3
Diameter	5.08	cm
NTD response	490	μV/MeV
Baseline resolution (RMS)	121 ± 2	eV
Peak σ at 5.9 keV	140 ± 8	eV

the K_α and K_β peaks of W at 59.3 keV and 67.2 keV, respectively, as well as the K_α line of Th at 93.3 keV, all originating from the thoriated tungsten wire γ-ray source. In addition to these three lines, the K_α line of lead at 74.7 keV is also visible.

Similarly, the Ge-LD data were processed to calibrate its energy spectrum using the ^{55}Fe source. The Ge-LD without applying the NTL-effect exhibits a baseline resolution of $\sigma_{RMS} = 60.4 \pm 0.5$ eV and a peaks resolution of $\sigma = 102 \pm 2$ eV. By exploiting the NTL-effect, the baseline resolution was improved by a factor of 12 reaching $\sigma_{RMS} = 5.2 \pm 0.1$ eV. Once the calibration of both detectors was completed, the data acquired with the NTL-effect enabled to study the scintillation light of GaAs. For each fired trigger in the heat channel, we simultaneously acquired the waveform in the Ge-LD data stream to investigate its corresponding signal. This allowed us to record coincident signals, thus producing a light versus heat scatter plot including all detected events, as shown in Fig. 4.

This separation is made possible by the different scintillation light yields associated with each type of interaction. From Fig. 4, we observe a clear separation of the two different families. In the α band, between 2 and 4.5 MeV, events from

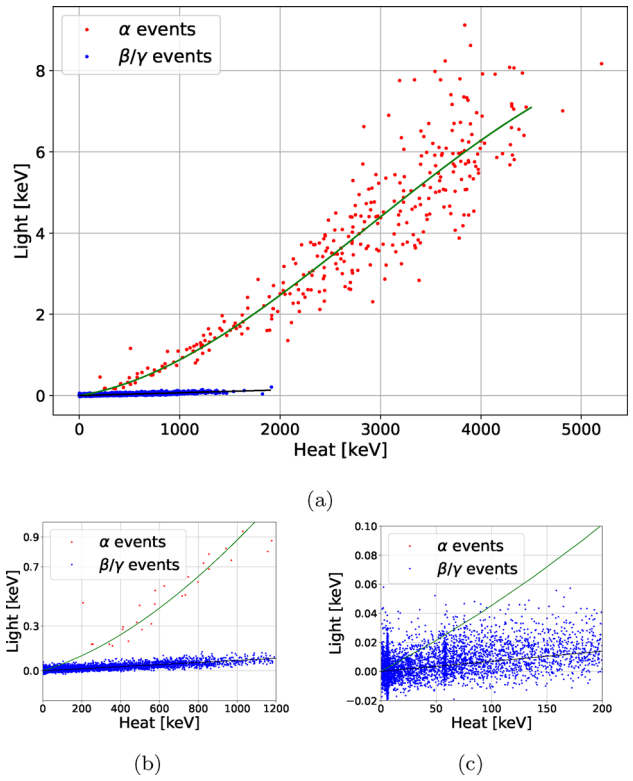

Fig. 4 (**a**) Light versus heat scatter plot constructed for events collected within the calibration run with the simultaneously installed ^{238}U α source and X-rays from ^{55}Fe and W. The population of β/γ and α events is highlighted in blue and red, respectively. See more information in the text below. (**b**) Zoom to show the evaluation of the LY at 1 MeV. (**c**) Zoom to show the low energy region

Table 3 Light yield values for β/γ and α induced events

	Light yield (keV/MeV) @ 1 MeV
β/γ	0.07 ± 0.01
α	0.9 ± 0.2

the ^{238}U source are observed. The α induced events appear smeared, and this can be explained by the use of a multi-layer deposited source and by irradiation of the non-polished surface of the GaAs-1 wafer by α particles.

Scintillation events induced by α particles were fitted using a third-degree polynomial function ($E_L = aE_H{}^3 + bE_H{}^2 + cE_H$), in order to highlight the non-linearity in the light yield (LY) response to this type of interaction. In contrast, events belonging to the β/γ band were fitted with a straight line ($E_L = a'E_H$). The fit coefficients obtained were $a = -0.06(2)$, $b = 0.54(1)$, and $c = 0.4(2)$ for the α events, and $a' = 0.069(1)$ for the β/γ events. The light energy (E_L) is expressed in keV, while the heat energy (E_H) is expressed in MeV.

The zoom of the light versus heat scatter plot for the energy interval from 6 keV to 1.2 MeV energy deposition in the heat channel is shown in Fig. 4b. From this figure and using energy dependence of light for β/γ events one can evaluate a number of photons emitted per keV, when GaAs excited by low-energy X-rays. Taking into account that emission maximum for the undoped GaAs crystal is 840 nm (1.476 eV) [25] the derived LY is 0.05 photon/keV.

Due to the absence of a clear and distinctive calibration α peaks of ^{238}U and strong non-linear behavior of the light yield (LY) induced by α particles in a wide energy interval, to estimate the LY of the GaAs crystal, We decided to compare the amount of light with the 1 MeV energy deposition measured in the heat channel. Moreover, it should be emphasised that because of the GaAs crystal geometry (a thin wafer weighing several grams) the energy scale for β/γ events was calibrated using X-rays peaks up to 60 keV (from ^{55}Fe and W) clearly visible in the energy spectrum, and assuming a linear detector response in the heat channel over a broader energy range. The zoom of the light versus heat scatter plot up to 1.2 MeV energy deposition in the heat channel is shown as inset in Fig. 4b, whilst the LY values for β/γ and α events estimated at 1 MeV energy deposition are reported in the Table 3. Additionally, it should be stressed that since the energy scale of the GaAs detector was calibrated with γ sources and we cannot perform a proper energy calibration for α induced events because of no evident peaks, the real energy of α events represented at 1 MeV on Fig. 4 can vary about 10–20% from this nominal value. However, the possible mismatch of the nominal deposited energy for these α events is within the uncertainty of the LY value determination.

As one can see from Fig. 4 and values listed in Table 3, events induced by α particles characterised by a higher value of LY with respect to β/γ events, by a factor of 10. This is not a typical LY behavior for scintillating crystals. With a few exceptions, typically the amount of light produced in interactions with α particles is lower than that for β/γs of the same energy, and varies in the range from 0.2 to 0.6 of that for the β/γ induced events, see [49]. This reduction in scintillation light emission for α particles is described as a Quenching Factor (QF), and it is commonly explained on the basis of a saturation effect of luminescence centers due to the high ionisation density that characterises the interaction of a heavy charged particle in matter [50,51]. However, as mentioned above, there are several exceptions amongst scintillating materials, for which QF > 1. The first amongst them is the ZnSe scintillating crystal for which QF > 1, yet the QF value is hardly reproducible and varies widely from one sample to another, reaching QF > 3–6 for some cases [52–55].

The second example is the ZnO crystal, for which in cryogenic measurements as a scintillating calorimeter, the light yield of events induced by α particles is higher than that of events induced by β/γ particles.

Similarly, the shape, intensity and energy position of the emission peaks, especially in the 800–900 nm wave-

Table 4 Summary of the performance of GaAs-2 detector operated as a low-temperature calorimeter

Mass	3.5	g
Density	5.32	g/cm^3
Diameter	5.08	cm
NTD response	1645	μV/MeV
Baseline resolution (RMS)	44.5 ± 0.8	eV
Peak σ at 5.9 keV	59 ± 1	eV

length interval, in GaAs crystals are reported to be strongly depended on the material chemical purity, type of dopants, defect structure, and on the type of conductivity, as shown in [25] and references therein.

In all above mentioned cases, such anomalous behavior of scintillation mechanism cannot be easily accommodated within the existing theoretical framework used to describe the scintillation properties of materials. Hence further investigations of this phenomenon, i.e. the light yield enhancement of α particles in GaAs crystal, are strongly required. Nevertheless, this feature is very important for particle discrimination, since when the light yield is a strong function of the particle type, the effective particle discrimination can be achieved.

4.2 GaAs-2 crystal

With the 3.5 g GaAs detector a 72-hour-long calibration run was performed, exposing the GaAs crystal only to a ^{55}Fe X-ray source. Data acquisition and analysis were performed using the same software framework previously employed.

As reported in Table 4, the baseline resolution was measured to be 44.5 ± 0.8 eV. Setting the threshold at 3σ results in a threshold energy of 133.5 eV, corresponding to an improvement in resolution by approximately a factor of three with respect to our previous work [48]. Furthermore, Fig. 5 clearly shows a distinct separation between the K_α and K_β Mn peaks, highlighting the enhanced performance of the detector. Since the ^{55}Fe X-ray calibration source was deposited on an aluminum foil and in the low-energy region E < 5 keV, as shown in the inset in Fig. 5, we identify the K_α peak of aluminum and a contribution from the K_α line of calcium.

The improved performance of the new GaAs crystal is likely related to its reduced mass, as in many bolometric detectors the performance scales with the absorber mass [56].

5 Conclusions and perspectives

The first successful measurements of the GaAs crystal as a cryogenic scintillating calorimeter with a dual readout (scintillation light and heat) were performed at the underground

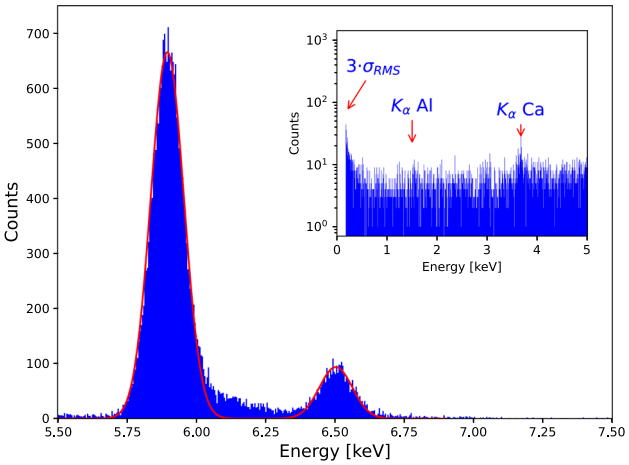

Fig. 5 The low-energy X-ray spectrum acquired with a 3.5 g GaAs detector and prominently featuring the 5.9 keV Mn K_α line and 6.49 keV K_β. Notably, the energy resolution at the 5.9 keV Mn K_α line peak is measured at σ = 59 ± 1 eV. This value was extracted from the fit of the spectrum using the sum of two Gaussian functions, one for the Mn K_α peak and one for the K_β peak, imposing the same sigma for both peaks

site of the Laboratori Nazionali del Gran Sasso (LNGS, Italy).

In the heat readout channel, the low-energy threshold of the 4.3 g GaAs detector was lowered from 1.5 keV to 360 eV, calculated as three times the baseline resolution, when compared to the previous measurements [48]. At the same time, the energy resolution at 5.9 keV X-ray peak was measured as 140 ± 8 eV. Both indicating significant improvement in noise and vibration reduction thanks to the latest modification of the IETI dilution refrigerator at LNGS.

In similar measurements with the 3.5 g GaAs detector equipped with the same Ge-NTD thermistor, the low-energy threshold was even further lowered to 133.5 eV, while 59 ± 1 eV of energy resolution was achieved for a 5.9 keV X-ray peak.

The results obtained are highly encouraging in view of the development of low-energy threshold high-resolution cryogenic detectors based on GaAs crystals, aimed at direct low-mass dark matter searches. Especially, when focusing on the detection channel involved electron scattering or dark photon absorption. Despite the current limitations imposed by the use of the Ge-NTD sensor for the heat channel readout, the observed detectors performance provides valuable insights for further optimising the GaAs detector design and experimental configuration.

Moreover, thanks to the simultaneously recording scintillation light with the cryogenic Ge-LD, the particle discrimination capability based on the different light response to the different type of irradiation has been demonstrated with the GaAs crystal for the first time. The light yield measured for β/γ induced events was evaluated at 0.07 ± 0.01 keV/MeV

(0.05 photons/keV). While the light yield estimated for α induced event exhibits 0.9 ± 0.2 keV/MeV, i.e. a factor of 10 more than for β/γ events. Such unusual luminescence properties of the GaAs crystal, i.e. producing more light when irradiated by α with respect to signals originated from β/γs of the same energy, is similar to features observed with ZnSe and ZnO scintillating crystals, and is a subject for further detailed studies. Since it can lead to a highly sensitive detection method for low-energy nuclear recoils as a result of light-mass DM particles scattering on Ga or As nuclei. Further investigations will focus on the unusual luminescence behavior, including using an alpha source with a better-defined peak to improve measurement accuracy. We will also optimize light collection efficiency and explore different source positioning configurations, enhancing sensitivity and providing a deeper understanding of the material's response. To further improve the low-energy threshold in the heat channel of the GaAs detector there are few possible options. One option would be to apply the NTL effect to a GaAs detector. Another option would be to adopt Transition Edge Sensors (TES) as thermal sensors for both heat and light signal readout, due to the fact that the logarithmic sensitivity of TES is roughly one order of magnitude higher than that of NTDs, resulting in a significantly improved signal-to-noise ratio. These advancements are expected to greatly enhance our measurement capabilities, extending the reach of direct dark matter detection and enabling the exploration of previously inaccessible regions of the dark matter parameter space.

Acknowledgements This work has been funded by the Italian University and Research Ministry thought the grant PRIN2022 – NextGenerationEU. We are particularly grateful to Dr. J. Walker Beeman for his invaluable support in the production of NTDs. We are also grateful to M. Guetti for the assistance in the cryogenic operations and the mechanical workshop of LNGS.

Data Availability Statement Data will be made available on reasonable request. [Author's comment: The datasets generated during and/or analysed during the current study are available from the corresponding author on reasonable request.].

Code Availability Statement Code/software will be made available on reasonable request. [Author's comment: The code/software generated during and/or analysed during the current study is available from the corresponding author on reasonable request.].

Funded by SCOAP[3].

References

1. B. Dutta, S. Ghosh, J. Kumar, Phys. Rev. D **100**, 075028 (2019). https://doi.org/10.1103/PhysRevD.100.075028
2. R. Essig, J. Mardon, T. Volansky, Phys. Rev. D **85**, 076007 (2012). https://doi.org/10.1103/PhysRevD.85.076007
3. J. Aalbers et al., Phys. Rev. D **108**(7), 072006 (2023). https://doi.org/10.1103/PhysRevD.108.072006
4. E. Aprile et al., Phys. Rev. Lett. **131**, 041003 (2023). https://doi.org/10.1103/PhysRevLett.131.041003
5. M. Rossi, Nuovo Cim. C **47**(3), 135 (2024). https://doi.org/10.1393/ncc/i2024-24135-7
6. C. Cheng et al., Phys. Rev. Lett. **126**(21), 211803 (2021). https://doi.org/10.1103/PhysRevLett.126.211803
7. C.A.J. O'Hare, Phys. Rev. Lett. **127**, 251802 (2021). https://doi.org/10.1103/PhysRevLett.127.251802
8. D.E. Kaplan, M.A. Luty, K.M. Zurek, Phys. Rev. D **79**, 115016 (2009). https://doi.org/10.1103/PhysRevD.79.115016
9. L.J. Hall, K. Jedamzik, J. March-Russell, S.M. West, JHEP **03**, 080 (2010). https://doi.org/10.1007/JHEP03(2010)080
10. Y. Hochberg, E. Kuflik, T. Volansky, J.G. Wacker, Phys. Rev. Lett. **113**, 171301 (2014). https://doi.org/10.1103/PhysRevLett.113.171301
11. E. Aprile et al., Phys. Rev. D **102**(7), 072004 (2020). https://doi.org/10.1103/PhysRevD.102.072004
12. J. Billard et al., Rep. Prog. Phys. **85**(5), 056201 (2022). https://doi.org/10.1088/1361-6633/ac5754
13. E. Aprile et al., Phys. Rev. Lett. **129**(16), 161805 (2022). https://doi.org/10.1103/PhysRevLett.129.161805
14. E. Aprile et al., (2024). arXiv:org/abs/2411.15289
15. D.S.E.A. Akerib, Phys. Rev. Lett. **122**, 131301 (2019). https://doi.org/10.1103/PhysRevLett.122.131301
16. D. Franco, in *57th Rencontres de Moriond on Electroweak Interactions and Unified Theories* (2023)
17. I. Arnquist et al., Phys. Rev. Lett. **130**(17), 171003 (2023). https://doi.org/10.1103/PhysRevLett.130.171003
18. Q. Arnaud et al., Phys. Rev. Lett. **125**(14), 141301 (2020). https://doi.org/10.1103/PhysRevLett.125.141301
19. P. Adari, I.M. Bloch, A.M. Botti, M. Cababie, G. Cancelo, B.A. Cervantes-Vergara, M. Crisler, M. Daal, A. Desai, A. Drlica-Wagner et al., Phys. Rev. Lett. **134**(1) (2025). https://doi.org/10.1103/physrevlett.134.011804. https://www.osti.gov/biblio/2282562
20. R. Agnese et al., Phys. Rev. Lett. **121**(5), 051301 (2018). https://doi.org/10.1103/PhysRevLett.121.051301 [Erratum: Phys. Rev. Lett. 122, 069901 (2019)]
21. T.K. Bui et al., Phys. Rev. Lett. **135**(16), 161002 (2025). https://doi.org/10.1103/hsrl-crvf
22. G. Angloher et al. (2025). arXiv:2505.01183
23. S. Derenzo, R. Essig, A. Massari, A. Soto, T.T. Yu, Phys. Rev. D **96**(1), 016026 (2017). https://doi.org/10.1103/PhysRevD.96.016026
24. S. Derenzo, E. Bourret, S. Hanrahan, G. Bizarri, J. Appl. Phys. **123**(11), 114501 (2018). https://doi.org/10.1063/1.5018343
25. S. Vasiukov, F. Chiossi, C. Braggio, G. Carugno, F. Moretti, E. Bourret, S. Derenzo, IEEE Trans. Nucl. Sci. **66**(11), 2333 (2019). https://doi.org/10.1109/TNS.2019.2946725
26. S. Pirro, P. Mauskopf, Annu. Rev. Nucl. Part. Sci. **67**, 161 (2017). https://doi.org/10.1146/annurev-nucl-101916-123130
27. S. Knapen, T. Lin, M. Pyle, K.M. Zurek, Phys. Lett. B **785**, 386 (2018). https://doi.org/10.1016/j.physletb.2018.08.064

28. S. Derenzo, R. Essig, A. Massari, A. Soto, T.T. Yu, Phys. Rev. D **96**, 016026 (2017). https://doi.org/10.1103/PhysRevD.96.016026
29. Y. Diakite, S. Traore, Y. Malozovsky, B. Khamala, L. Franklin, D. Bagayoko, J. Mod. Phys. **08** (2016). https://doi.org/10.4236/jmp.2017.84035
30. V. Zema et al., arXiv:2402.01395 (2024)
31. S. Knapen, J. Kozaczuk, T. Lin, Phys. Rev. D **105**(1), 015014 (2022). https://doi.org/10.1103/PhysRevD.105.015014
32. S. Knapen, J. Kozaczuk, T. Lin, Phys. Rev. D **105**, 015014 (2022). https://doi.org/10.1103/PhysRevD.105.015014
33. R. Essig et al., in *Snowmass 2021* (2022)
34. S. Griffin, S. Knapen, T. Lin, K.M. Zurek, Phys. Rev. D **98**(11), 115034 (2018). https://doi.org/10.1103/PhysRevD.98.115034
35. S. Pirro, C. Arnaboldi, J. Beeman, G. Pessina, Nucl. Instrum. Methods Phys. Res. Sect. A Accel. Spectrom. Detect. Assoc. Equip. **559**(2), 361 (2006)
36. J. Beeman, F. Bellini, N. Casali, L. Cardani, I. Dafinei, S. Di Domizio, F. Ferroni, L. Gironi, S. Nagorny, F. Orio et al., J. Instrum. **8**(07), P07021 (2013)
37. B.S. Neganov, V.N. Trofimov, Otkryt. Izobret. **146**, 215 (1985)
38. P.N. Luke, J. Appl. Phys. **64**(12), 6858 (1988). https://doi.org/10.1063/1.341976
39. Sigma-Aldrich. Sigma-Aldrich official website. https://www.sigmaaldrich.com/HK/en
40. E.E. Haller, N.P. Palaio, M. Rodder, W.L. Hansen, E. Kreysa, pp. 21–36 (1984). https://doi.org/10.1007/978-1-4613-2695-3_2
41. M. Barucci, V. Martelli, G. Ventura, J. Low Temp. Phys. **157**, 541 (2009). https://doi.org/10.1007/s10909-009-9981-0
42. C. Arnaboldi, P. Carniti, L. Cassina, C. Gotti, X. Liu, M. Maino, G. Pessina, C. Rosenfeld, B. Zhu, J. Instrum. **13**(02), P02026 (2018). https://doi.org/10.1088/1748-0221/13/02/P02026
43. P. Carniti, C. Gotti, G. Pessina, Nucl. Instrum. Meth. A **1045**, 167658 (2023). https://doi.org/10.1016/j.nima.2022.167658
44. A. Armatol, B. Broerman, L. Dumoulin, A. Giuliani, H. Khalife, M. Laubenstein, P. Loaiza, P. De Marcillac, S. Marnieros, S. Nagorny et al., J. Instrum. **18**(06), P06026 (2023)
45. A. Armatol, E. Armengaud, W. Armstrong, C. Augier, F. Avignone III., O. Azzolini, I. Bandac, A. Barabash, G. Bari, A. Barresi et al., J. Instrum. **16**(02), P02037 (2021)
46. Gnu octave. https://www.octave.org/
47. E. Gatti, P.F. Manfredi, Riv. Nuovo Cim. **9N1**, 1 (1986). https://doi.org/10.1007/BF02822156
48. D.L. Helis, A. Melchiorre, A. Puiu, G. Benato, P. Carniti, A. Continenza, N. Di Marco, A. Ferella, C. Ferrari, F. Giannessi, C. Gotti, E. Monticone, L. Pagnanini, G. Pessina, S. Pirro, G. Profeta, M. Rajteri, P. Settembri, A. Shaikina, C. Tresca, D. Trotta, Eur. Phys. J. C **84**(7), 749 (2024). https://doi.org/10.1140/epjc/s10052-024-13123-8
49. D. Poda, Physics **3**(3), 473 (2021)
50. J.B. Birks, Proc. Phys. Soc. Sect. A **64**(10), 874 (1951)
51. V. Tretyak, Astropart. Phys. **33**(1), 40 (2010). https://doi.org/10.1016/j.astropartphys.2009.11.002. https://www.sciencedirect.com/science/article/pii/S0927650509001650
52. C. Arnaboldi, S. Capelli, O. Cremonesi, L. Gironi, M. Pavan, G. Pessina, S. Pirro, Astropart. Phys. **34**(6), 344 (2011)
53. J. Beeman, F. Bellini, L. Cardani, N. Casali, I. Dafinei, S. Di Domizio, F. Ferroni, L. Gironi, A. Giuliani, S. Nagorny et al., J. Instrum. **8**(05), P05021 (2013)
54. D. Artusa, A. Balzoni, J. Beeman, F. Bellini, M. Biassoni, C. Brofferio, A. Camacho, S. Capelli, L. Cardani, P. Carniti et al., Eur. Phys. J. C **76**, 1 (2016)
55. S. Nagorny, L. Cardani, N. Casali, I. Dafinei, L. Pagnanini, L. Pattavina, S. Pirro, K. Schaeffner, I.O.P. Conf, Ser. Mater. Sci. Eng. **169**, 012011 (2017)
56. R. Strauss, J. Rothe, G. Angloher, A. Bento, A. Gütlein, D. Hauff, H. Kluck, M. Mancuso, L. Oberauer, F. Petricca, F. Pröbst, J. Schieck, S. Schönert, W. Seidel, L. Stodolsky, Phys. Rev. D **96**, 022009 (2017). https://doi.org/10.1103/PhysRevD.96.022009